Chapter 12

Case Studies

This chapter presents several case studies showing the effects of various operational conditions.

Salt Flood and Body Insert

Figure 12-1 shows several examples of using short-offset salt floods to quickly determine the top and base of complex salt structures. In this case, the offset was limited to 1000 meters and a common azimuth algorithm was used to produce the image.

Figure 12-1. Short offset poststack salt Floods.

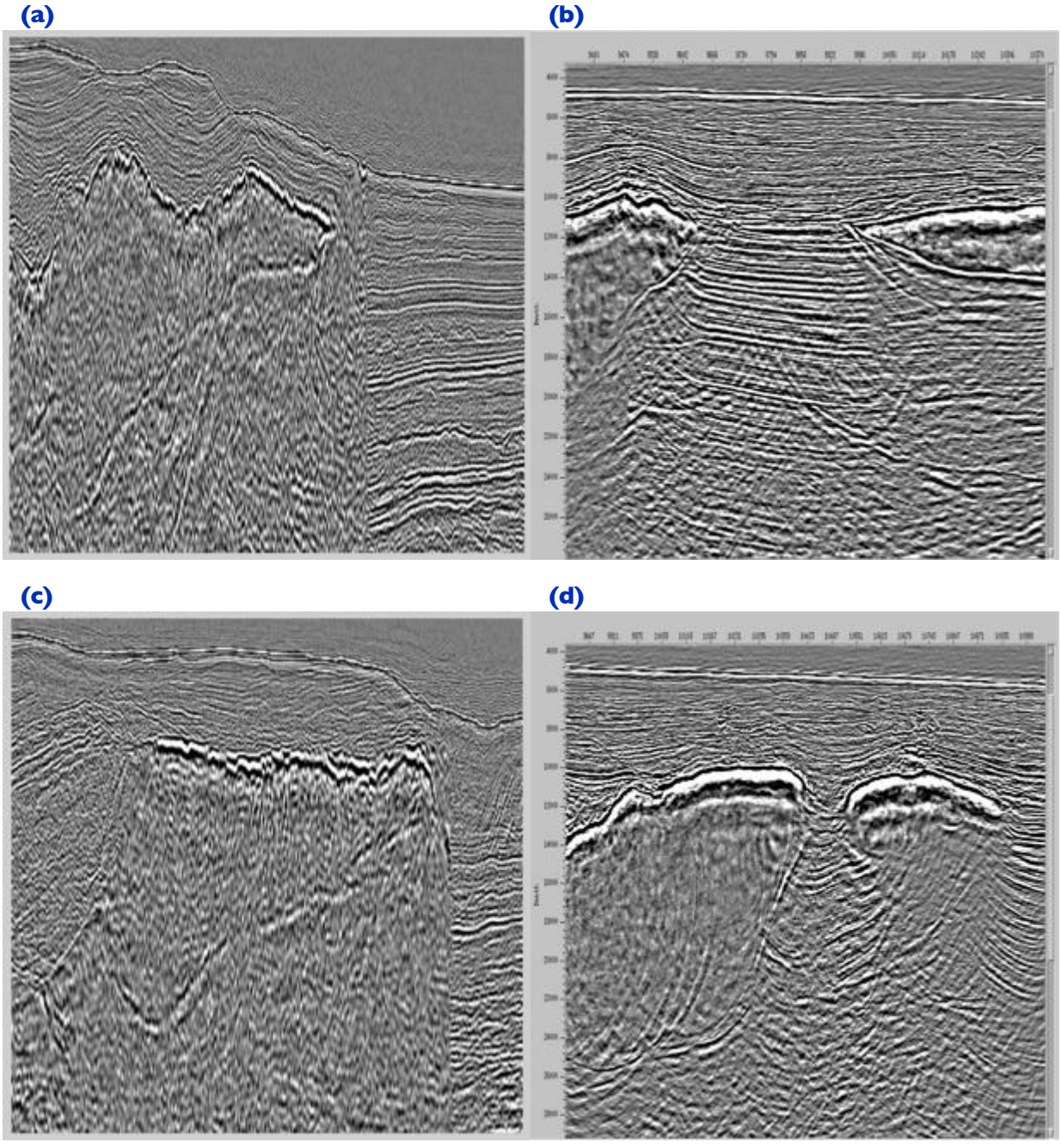

Each of these snapshots is from a Gulf of Mexico salt structure province and indicates the kinds of problems and issues that arise in this setting. Note that interpreting the top and base of salt is quite easy here, but that is not always the case. A major unsolved problem concerns why the salt base is not always visible.

Figure 12-2 shows a full volume image of a Gulf of Mexico salt structure after completion of detailed MVA and salt body insert. In this image, the salt base and sub-salt sediments are clearly imaged.

Figure 12-2. Full prestack Kirchhoff volume after salt body insert.

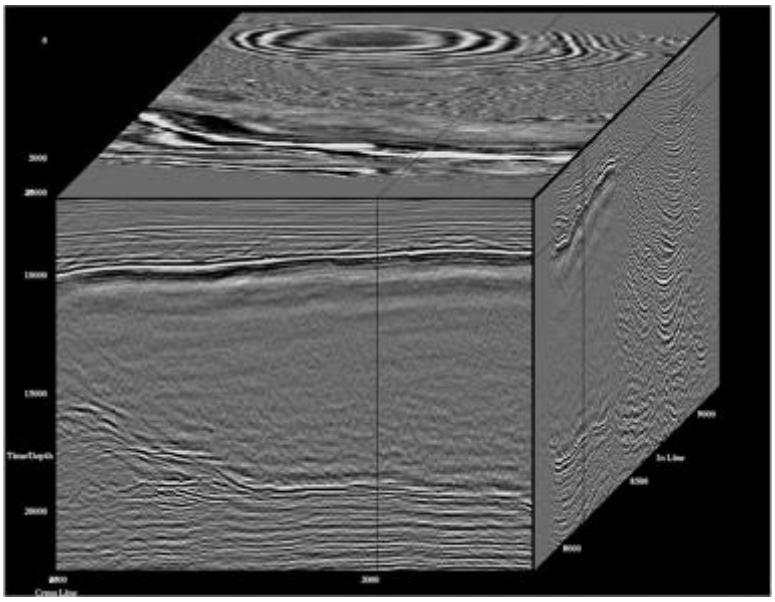

Comparing Figure 12-3(a) with (b), we observe excessive aliasing of the common azimuth section. This is very likely because the processor failed to properly assess and limit the input frequency content.

Figure 12-3. Wave Equation Aliasing

(a). Kirchhoff prestack xline image from the volume in Figure 12-2

(b). Common azimuth xline image from the volume in Figure 12-2

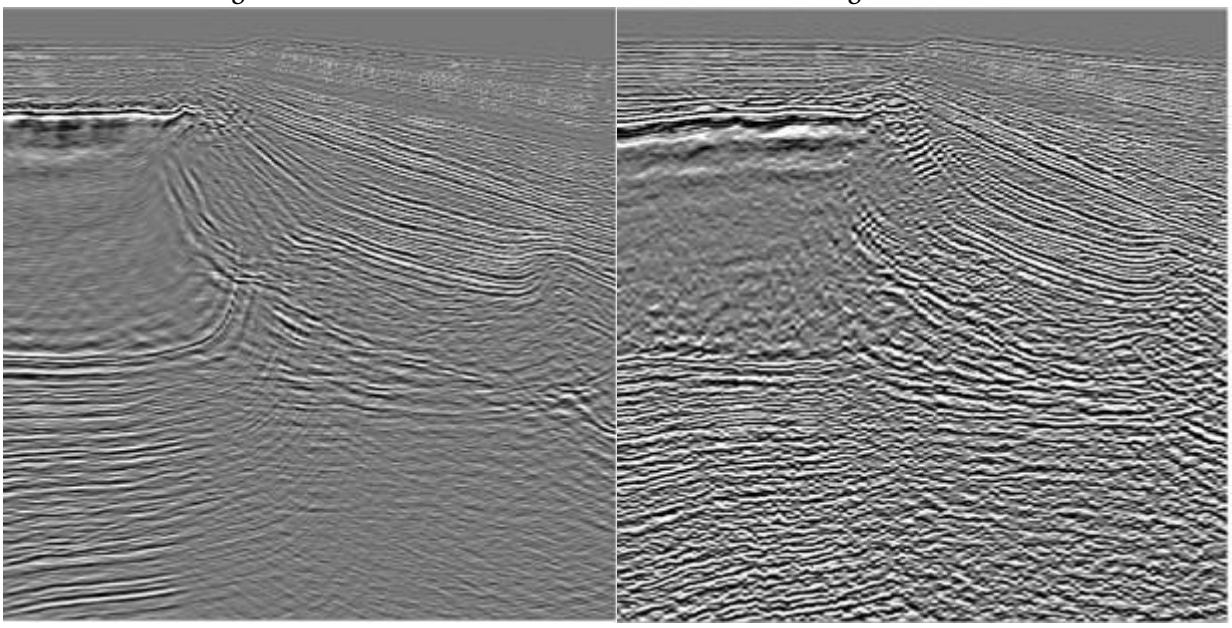

The two graphics in Figure 12-4 show that defining salt body shapes precisely when two salt structures almost overlap can be quite difficult.

Figure 12-4. Multi-level salt structures

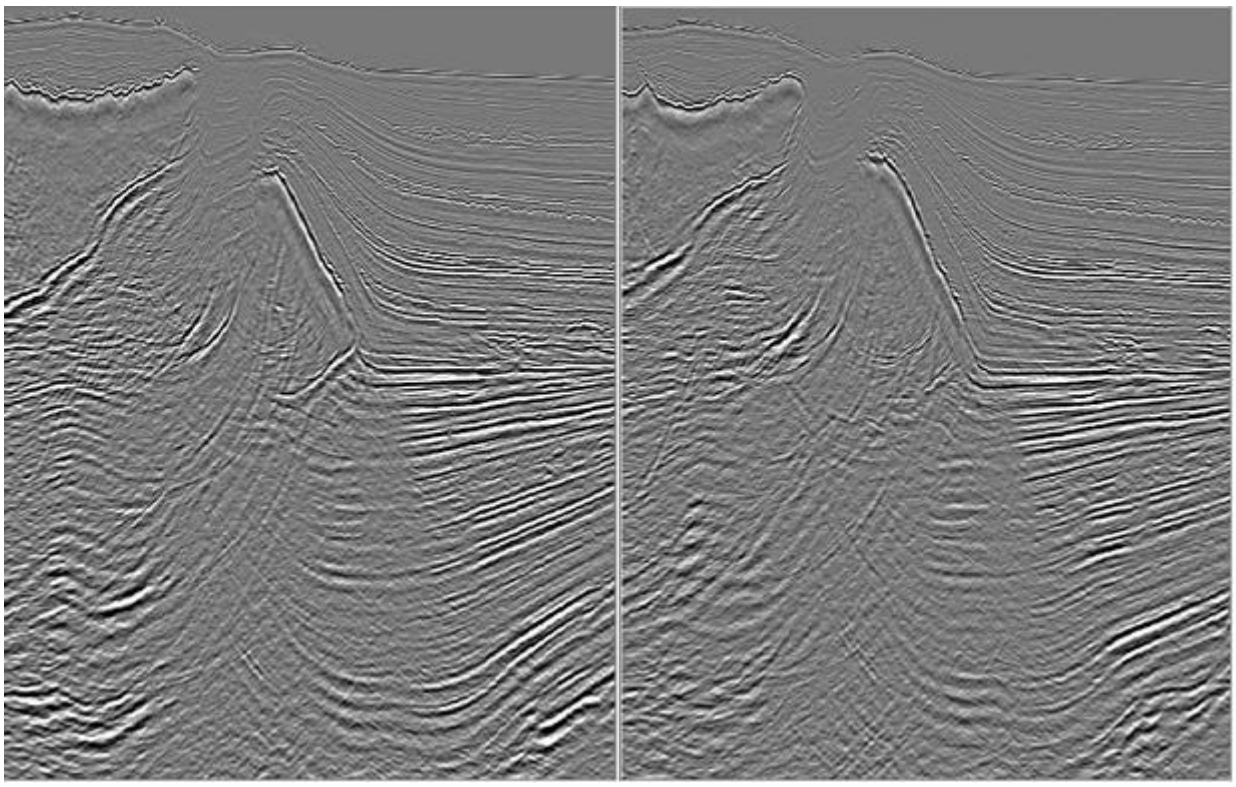

Salt structures, like the one in Figure 12-5, are relatively easy to image with single arrival Kirchhoff migrations. This is mostly due to the rugosity of the top of the salt.

Figure 12-5. Deep water laminate salt Kirchhoff imaging.

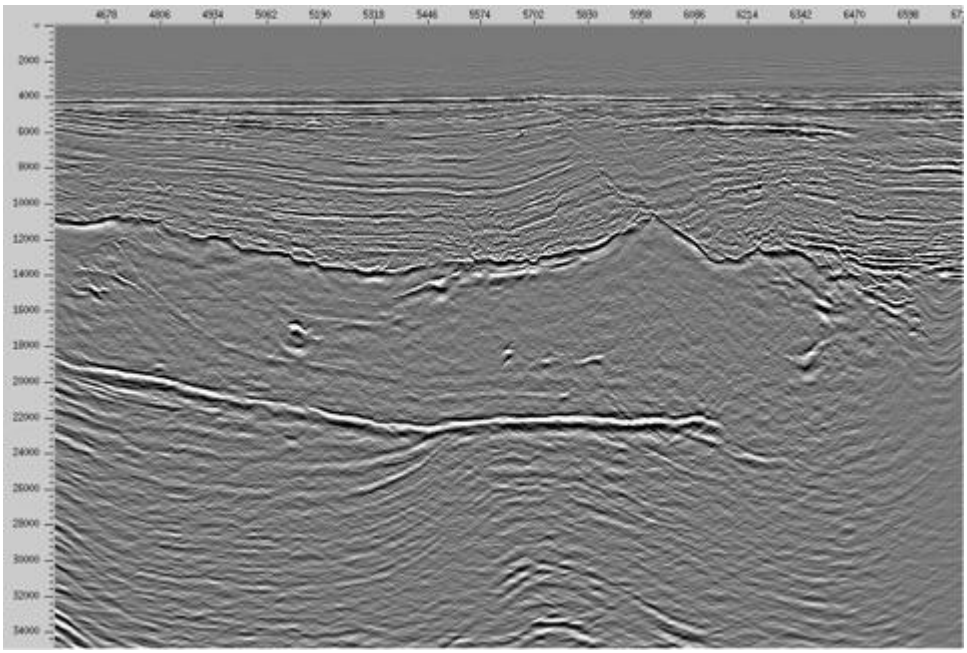

Amplitude Preservation

Figure 12-6 shows the relative amplitude differences between a full Kirchhoff migration (left) and a one-way phase-screen prestack depth migration (right).

Figure 12-6. Kirchhoff versus one-way shot profile offshore Florida

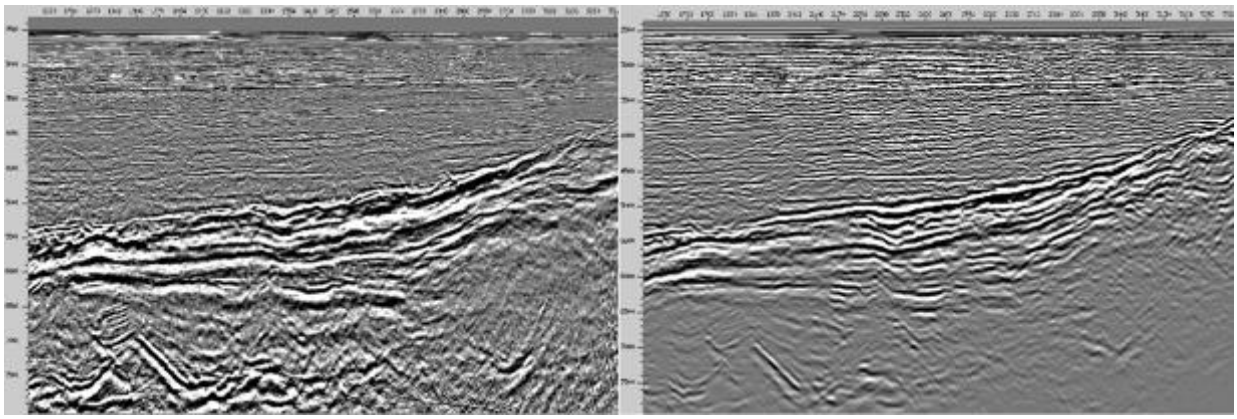

Which One Should I Use?

Figure 12-7. Inline slices through impulse responses

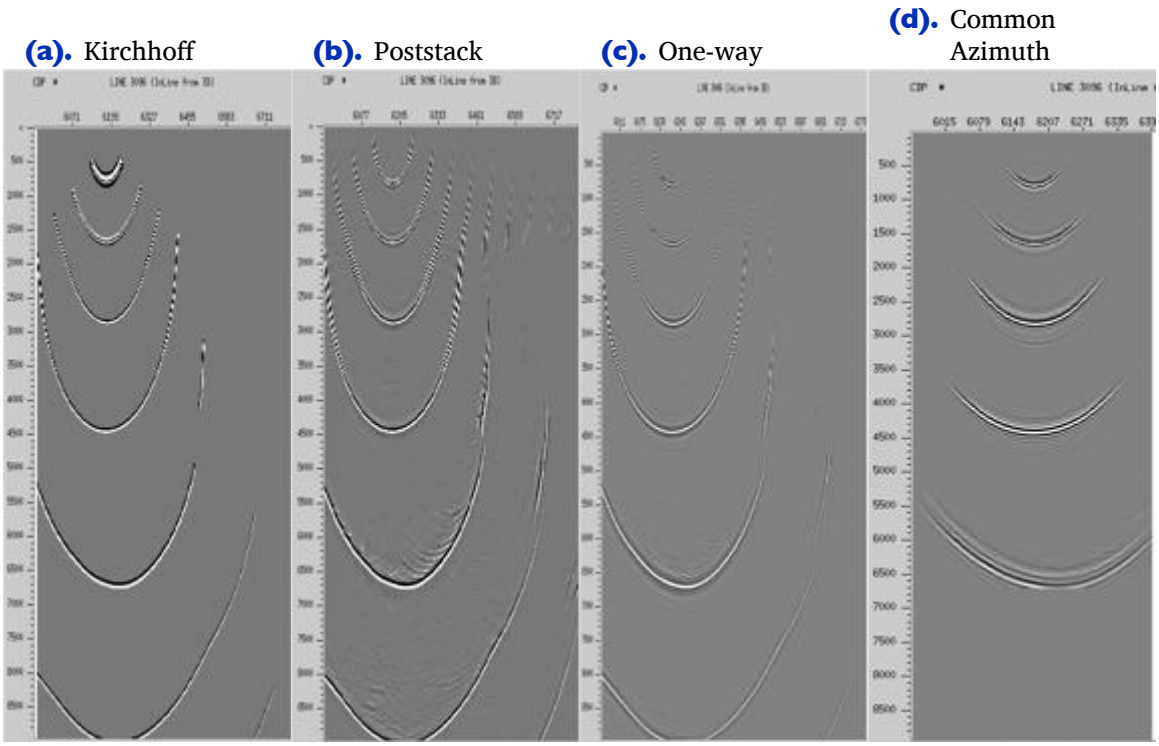

Figure 12-8. Crossline Slice Through Impulse Responses

(a). Kirchhoff **(b).** Poststack **(c).** One-way **(d).** Common Azimuth

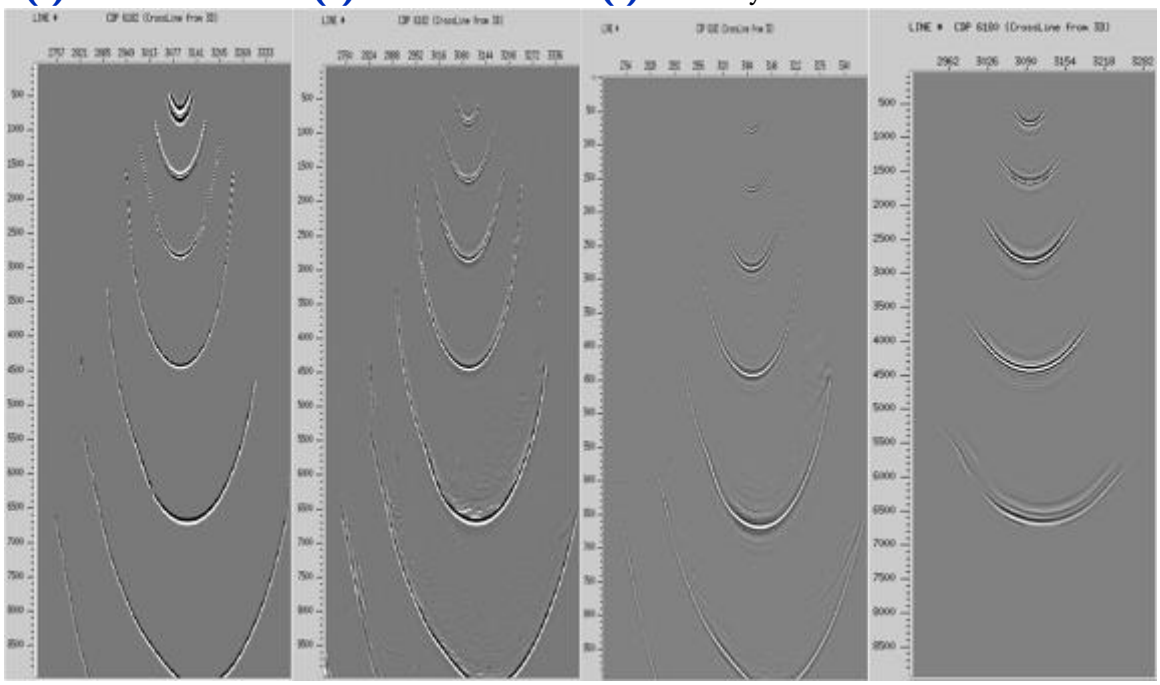

Figure 12-9. Depth slice through impulse responses

(a). Kirchhoff **(b).** Poststack **(c).** One-way **(d).** Common Azimuth

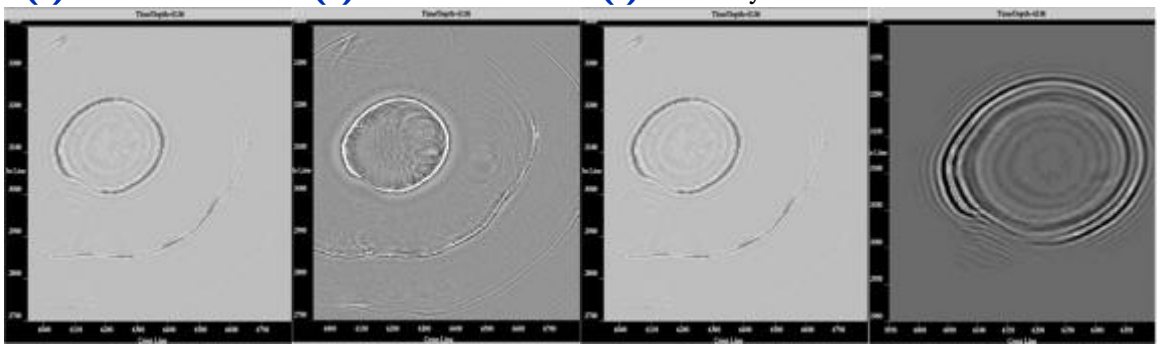

Land Data PSTM Versus PSDM Comparison

Figures 12-10, 12-11, 12-12, and 12-13, are examples from a 3D land survey near Daxing, China. What they all show is that wave equation migration is generally better at fault definition than single arrival based Kirchhoff methods. It is also much better at amplitude preservation, even when, as in the one way case, it is not perfect.

Figure 12-10. PSTM (top) versus PSDM (bottom) on land data near Daqing China

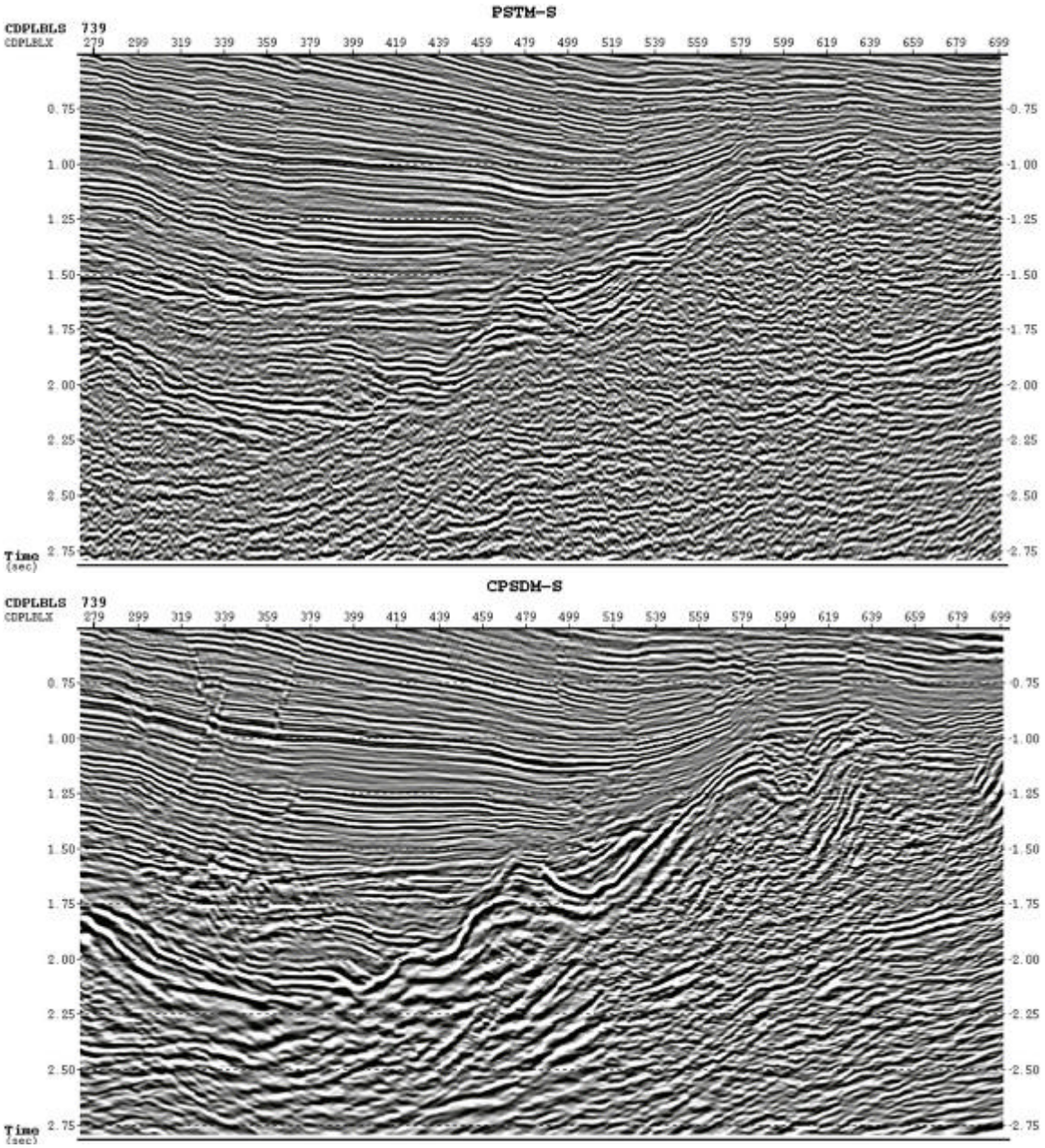

Figure 12-11. PSTM (top) versus PSDM (bottom) on land data near Daqing China

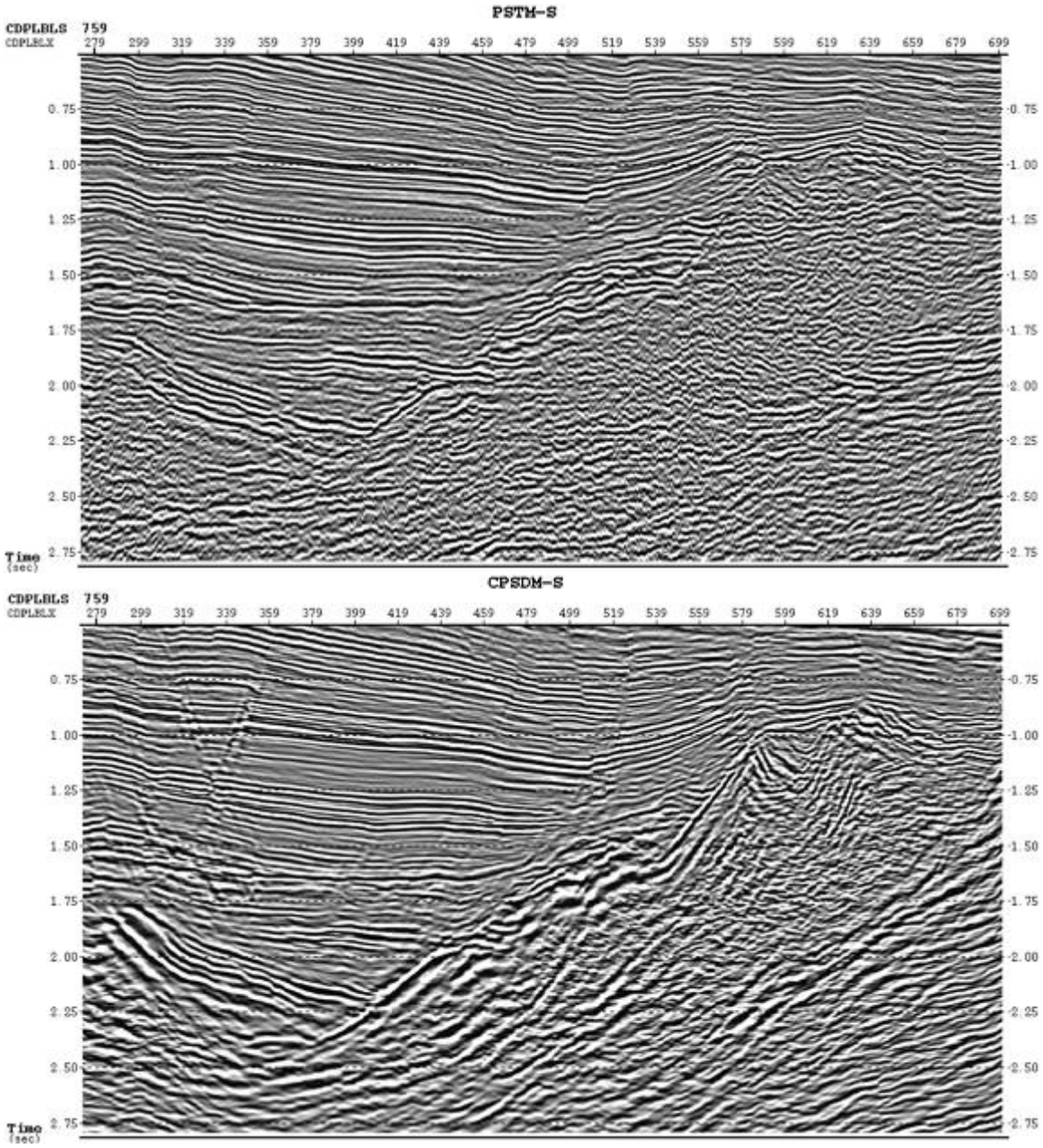

Figure 12-12. PSTM (top) versus PSDM (bottom) on land data near Daqing China

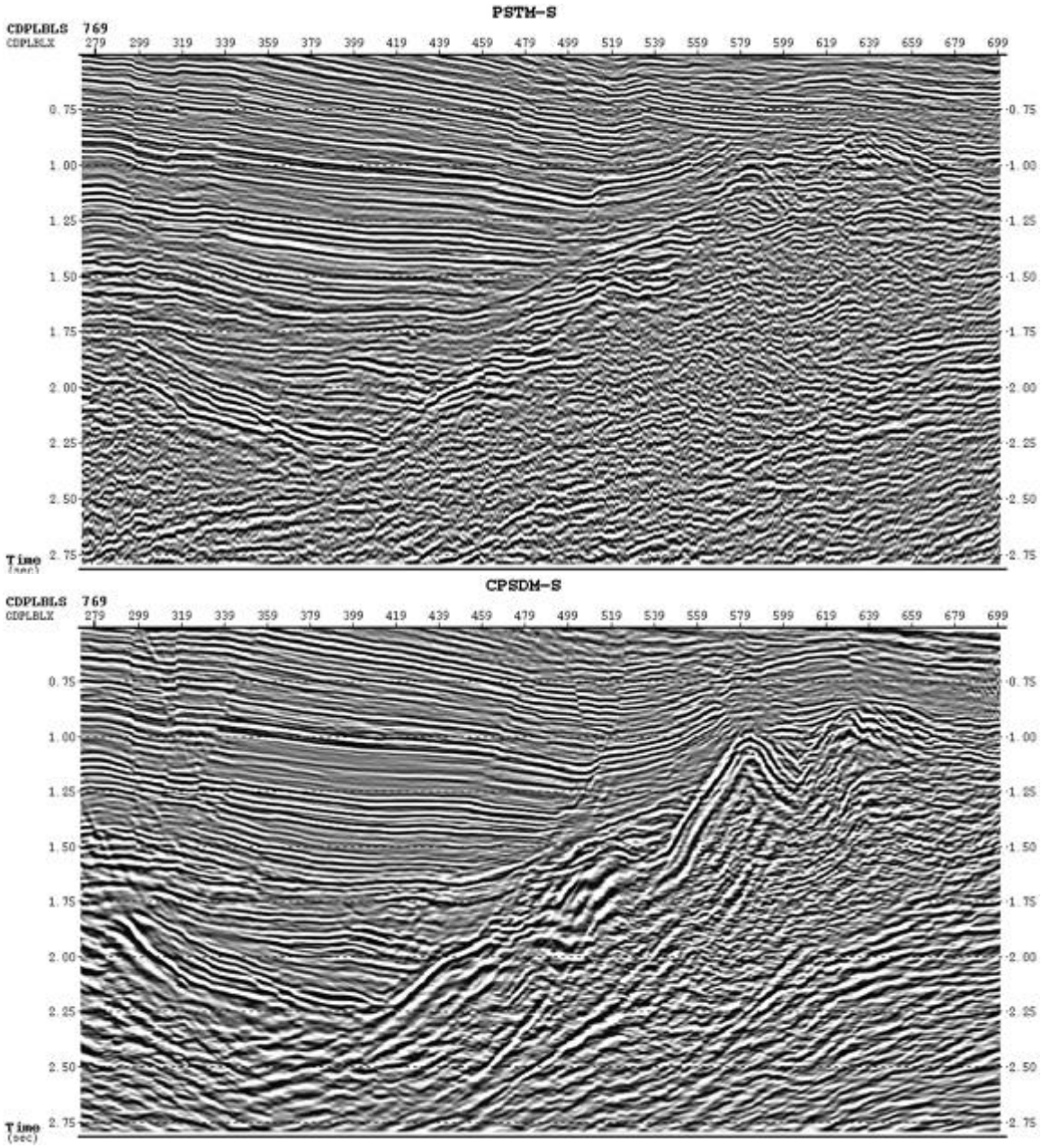

Figure 12-13 shows that when the data is over tertiary soft rock geology, the difference between various migration algorithms can be small. While certain parts of the top figure are better than the bottom figure, seeing the differences requires a sharp eye.

Figure 12-13. Curved ray PSTM versus Straight Ray on land data near Daqing China

(a). Curved Ray Kirchhoff PSTM

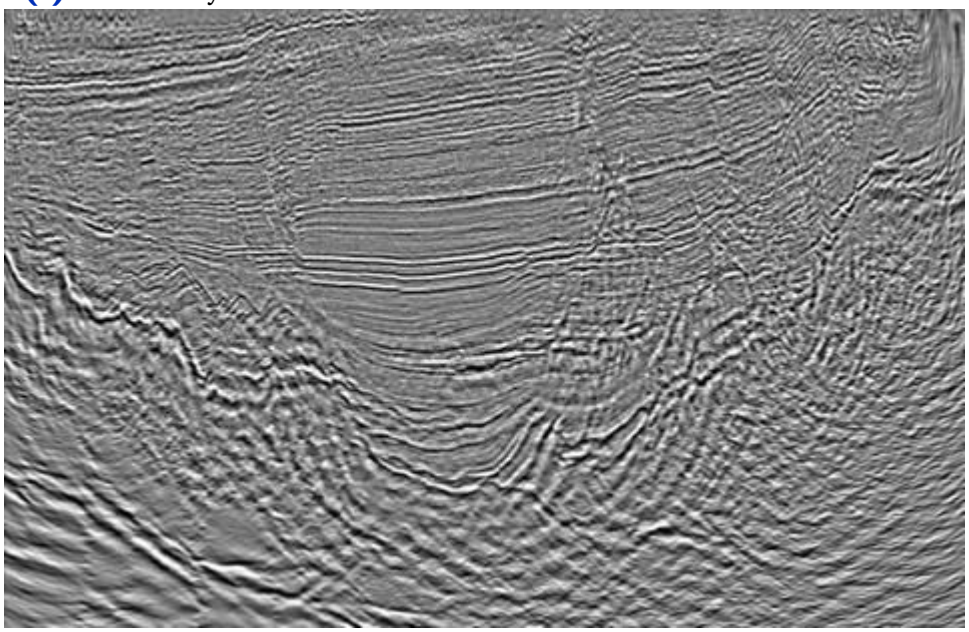

(b). Straight Ray Kirchhoff PSTM

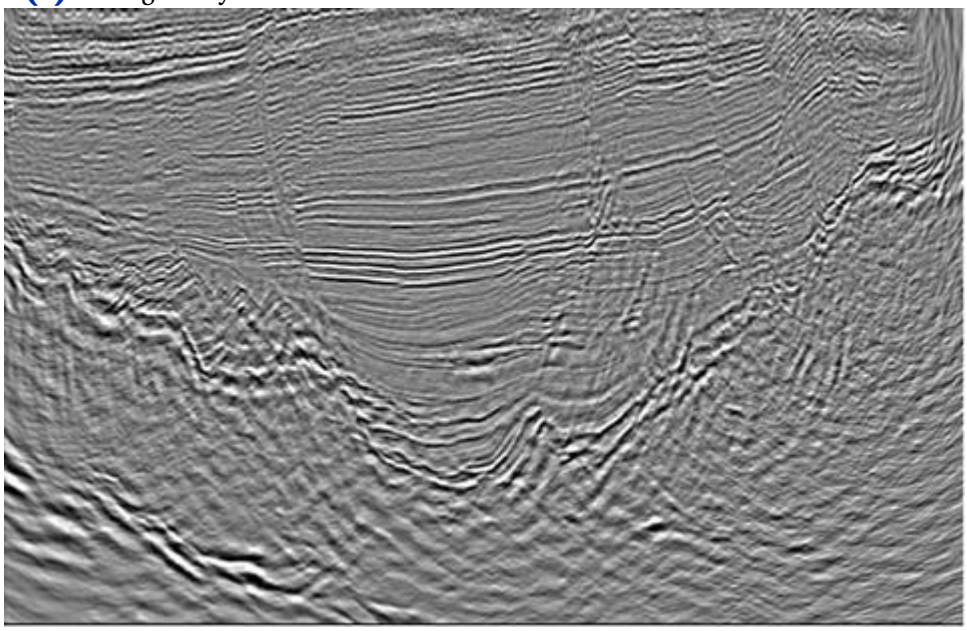

Autopicking PSTM

Figure 12-14 shows an image based on automatically picked velocities. In the image, the chase was the initial iteration of the imaging project.

Figure 12-14. Automatically picked and imaged PSTM

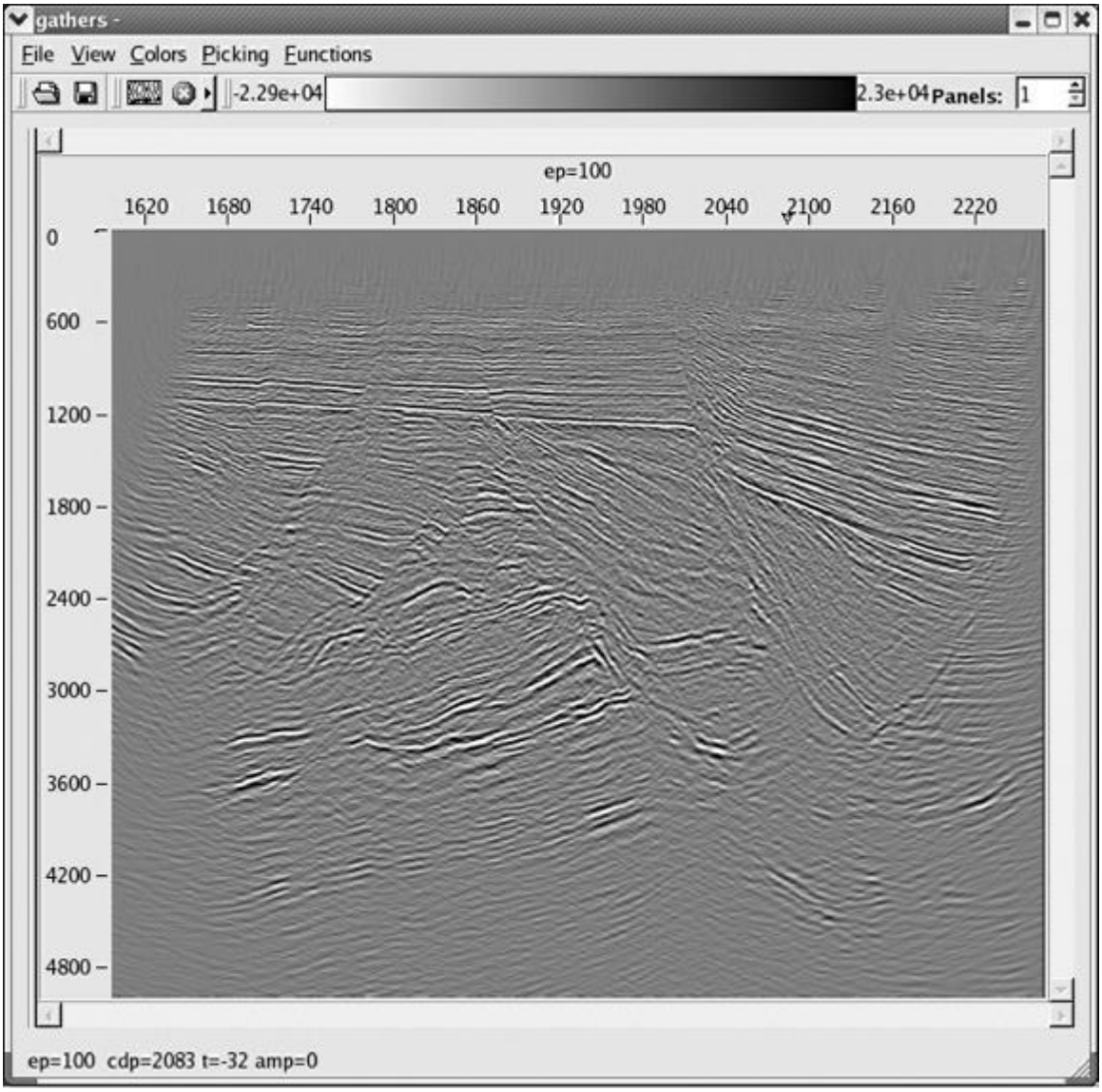

Tomography

Figure 12-15. A comparison of imaging with and without tomography

(a). Before tomography (left) and after tomography (right)

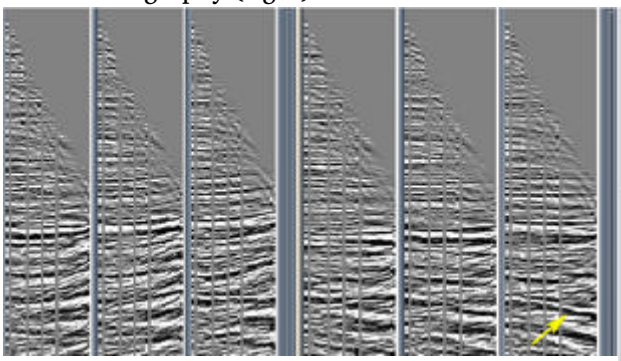

(b). Before tomography

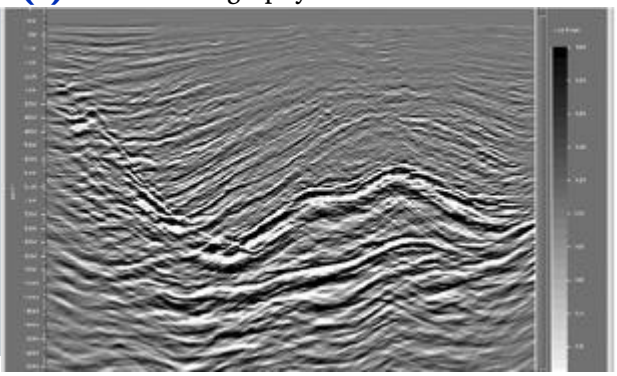

(c). After tomography

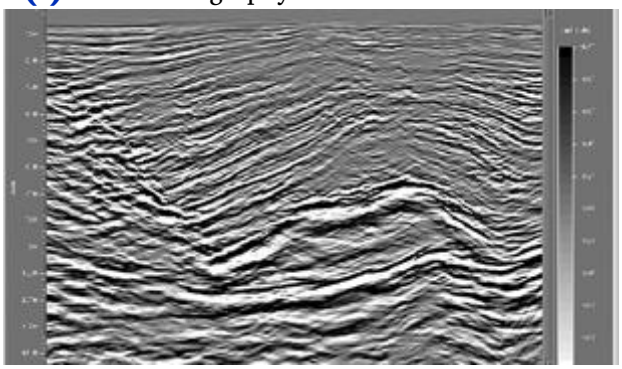

South Texas Fault Shadow

Figure 12-16(a) is a Kirchhoff PSTM that revealed a severe fault shadow imaging problem. Figure 12-16(b) shows that, while depth migration has generally improved the overall imaging quality, it has not completely solved the problem.

Figure 12-16. South Texas fault shadow

(a) South Texas fault shadow PSTM

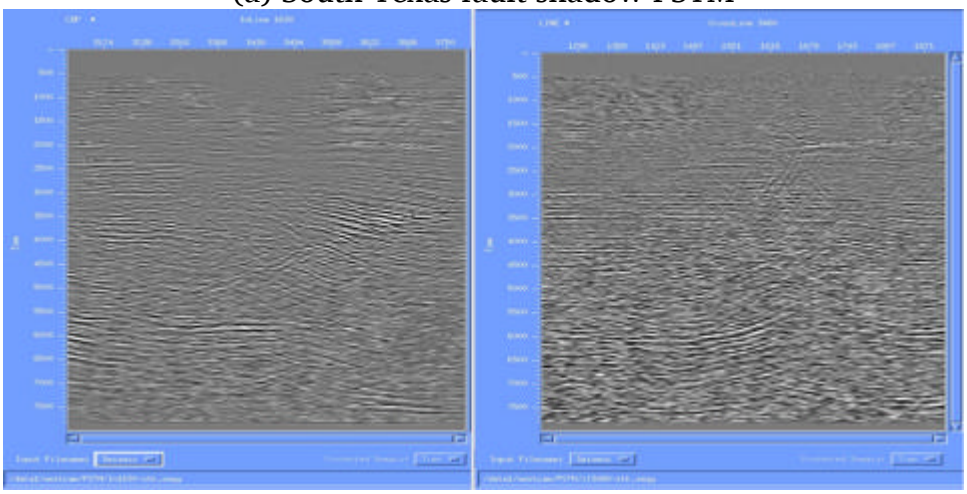

(b) South Texas fault shadow PSDM

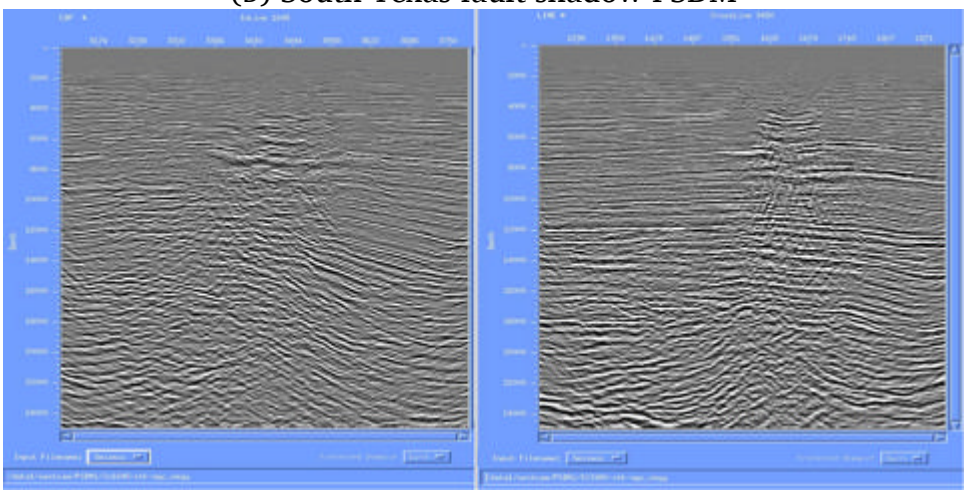

Blessing Texas Case Study

The availability of a small 3D Southeastern Texas Gulf of Mexico survey provided an excellent data set for directly comparing single arrival Kirchhoff migration with the much more computationally intensive full waveform reverse time migration. This study concluded that while there is an almost imperceptible difference between vertical time or depth sections, a high resolution fault analysis indicates that the more accurate method produces much higher resolution results. That this is the case, even when neither the geology nor the velocity model indicates any significant lateral gradients, is a bit surprising.

Figure 12-17 is a graphic montage depicting a 3D seismic survey acquired in the late 1980's or early 1990's near the town of Blessing in the state of Texas in the USA. The graphic in (a) shows the approximate location of the survey, (b) shows the CDP locations and fold, (c) shows the shot locations, and (d) shows an example shot where each shot was acquired by eight lines of receivers. There were approximately 1080 receivers per shot, and there were approximately 4265 shots. There are approximately 4,200,000 total traces in this survey.

Figure 12-17. Description of a 3D seismic survey Southwest of Houston near Blessing, Texas

(a). Blessing, Texas 3D survey location

(b). 3D CDP locations and Fold Map

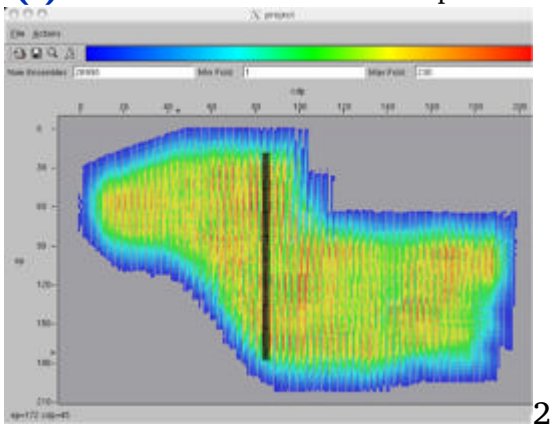

2

(c). Shot location map

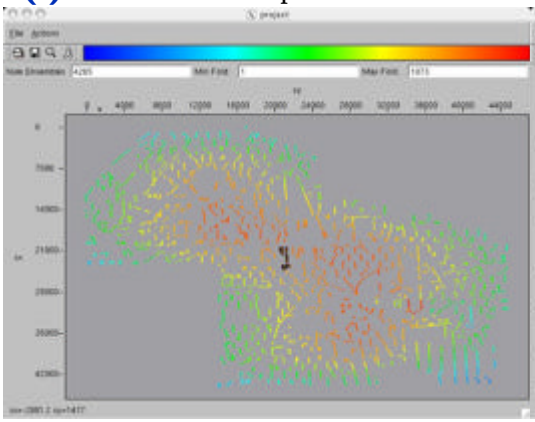

(d). Example shot record with 8 receiver spreads

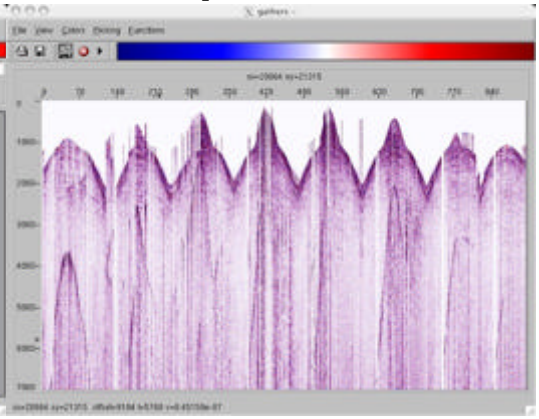

The migration in Figure 12-18 was one of the first done on the Blessing data. The target is indicated by the yellow square and the question was whether or not this clearly faulted zone contained one or two faults. A secondary question focused on whether the black square does or does not contain a continuation of the fault entering the square at the lower left corner.

Figure 12-18. A early Kirchhoff prestack depth migration of the Blessing data

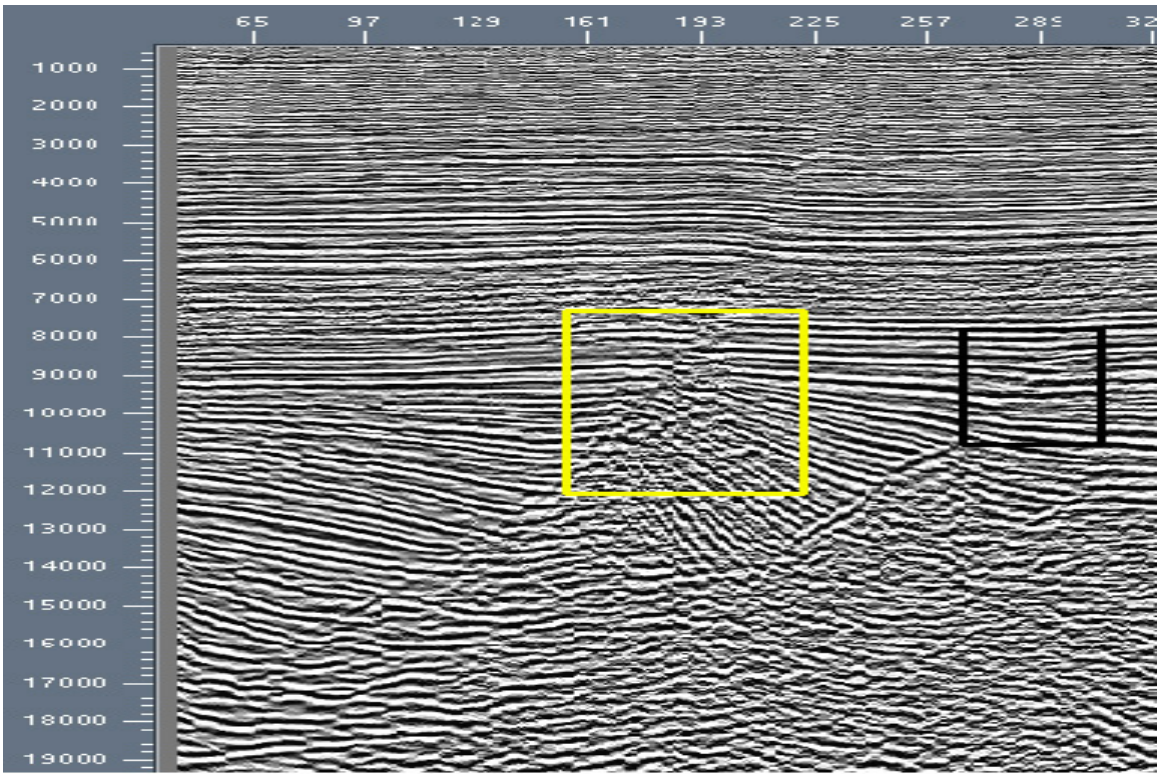

Figure 12-19(a) shows a straight ray time migration using the first iteration of velocity analysis, while (b) shows the second iteration result. Each of these initial iterations were performed using a semblance-based automatic picking routine. Figure 12-19(c) shows a curved ray PSTM with the final interval velocity volume. Part (d) is different because it used a migration algorithm that selected a velocity function at the source and another velocity function at the receiver to estimate the required traveltimes.

Figure 12-19. Four prestack time migrations of the 3D Blessing data

(a). Straight ray Kirchhoff with first velocity model

(b). Straight ray Kirchhoff with second velocity model

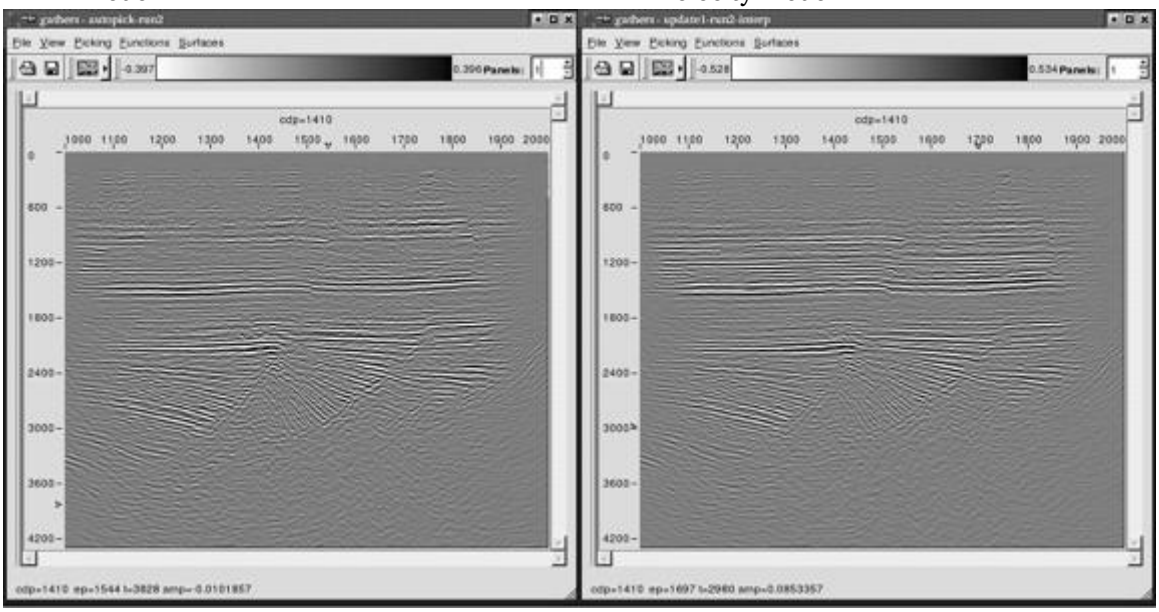

(c). Curved ray Kirchhoff with final velocity model

(d). Curved ray SR Kirchhoff with final velocity model

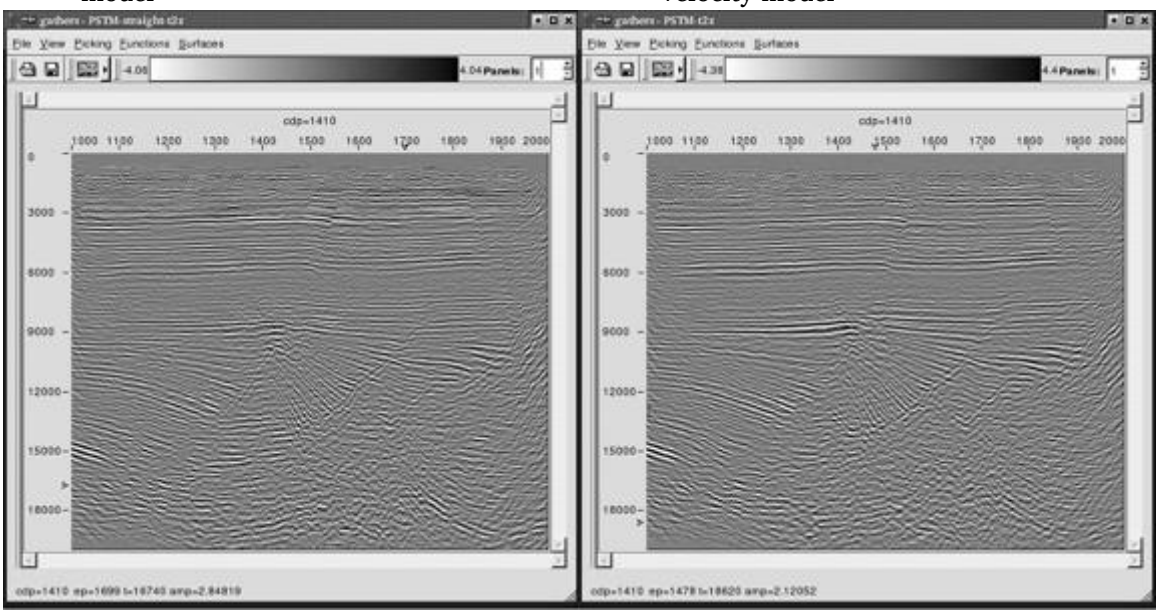

To ensure the highest possible velocity accuracy, tomography was applied to the Blessing data set. The before and after common image gather comparison in Figure 12-20 demonstrates that the painless velocity update method was sufficient to ensure high quality imaging.

Figure 12-20. A before and after comparison of tomography

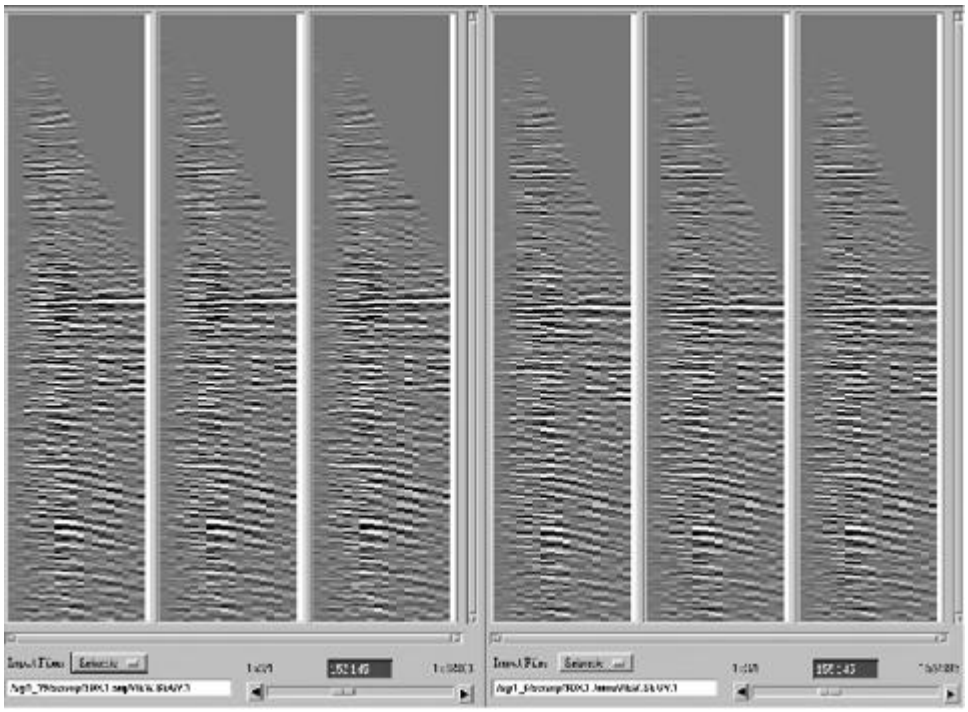

The images in Figure 12-21 represent the final depth-interval velocity volume and the final Kirchhoff maximum energy depth image at approximately line 1466.

Figure 12-21. Blessing Velocity Model and Kirchhoff PSDM

(a). Blessing interval velocity model

(b). Kirchhoff depth migration using the model in (a)

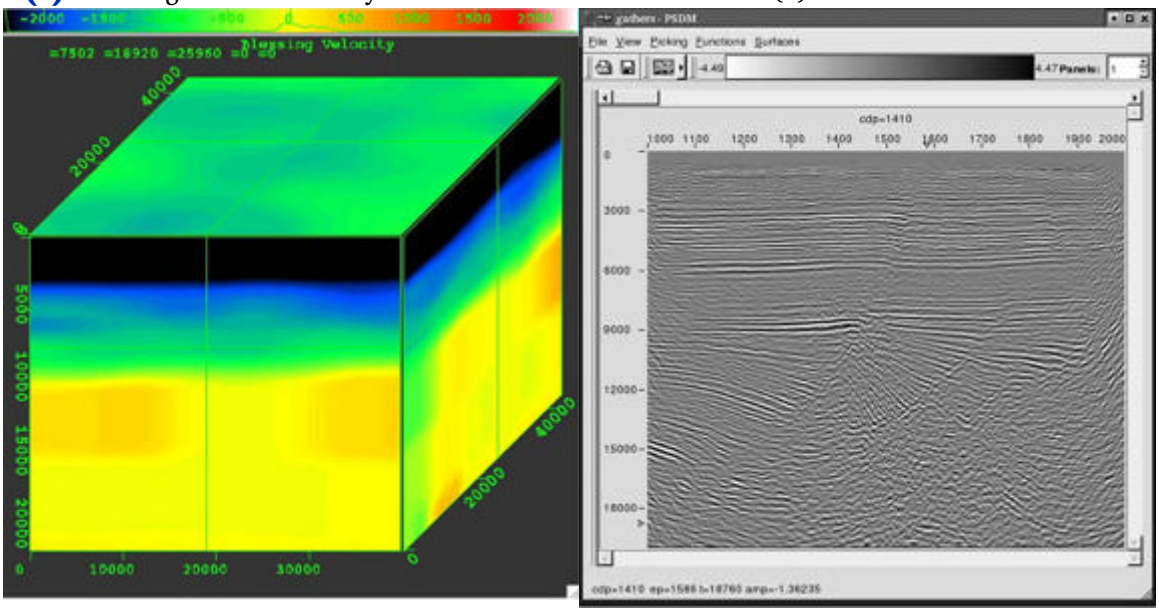

The key points of the images in Figure 12-22 are that, when viewed in sectional form, there appears to be little difference between the Kirchhoff single arrival in (a) and the much more computationally intensive reverse-time migration in (b). However, when viewed purely as depth slices, as in (c) and (d), the differences between the two methods are clear.

Figure 12-22. A Kirchhoff and Two-Way PSDM Comparison

(a). Kirchhoff PSDM and depth slice

(b). Two-way PSDM and depth slice

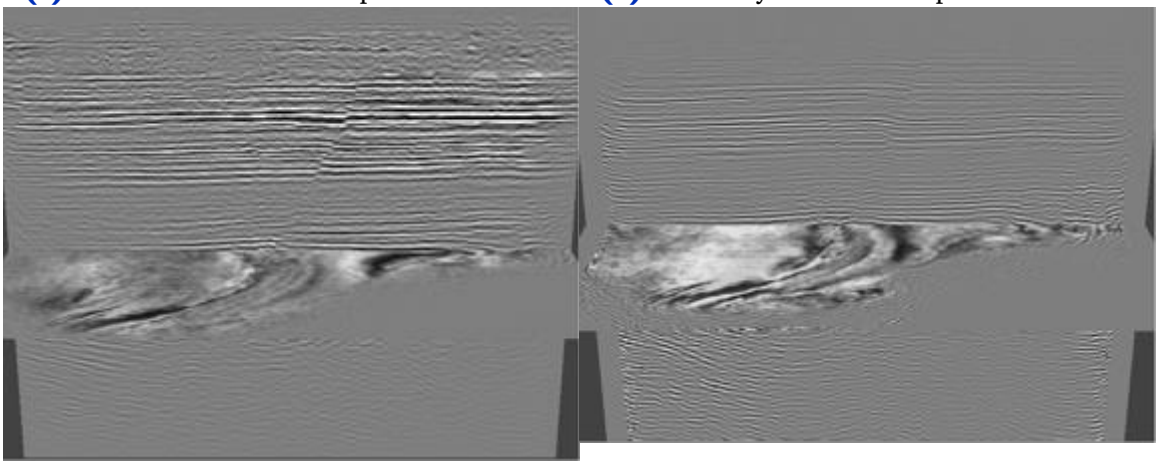

(c). Kirchhoff depth slice

(d). Two-way depth slice

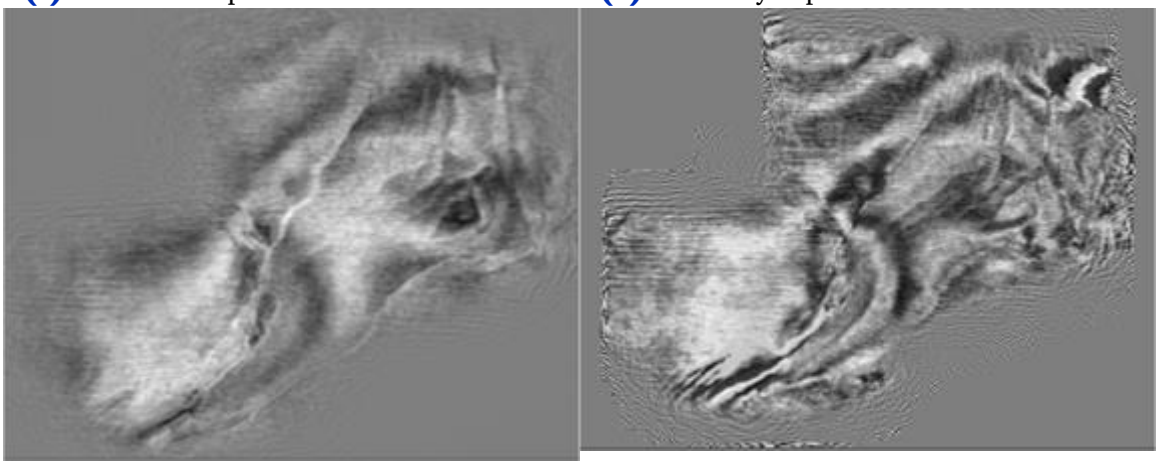

A high resolution fault analysis was run on both the Kirchhoff migration and the two-way volumes to verify the preliminary conclusion that the two-way method is of considerably higher resolution. A visual comparison of Figure 12-23(a) with Figure 12-23(b) confirms this basic hypothesis.

Figure 12-23. A high resolutions fault analysis of depth slices from a Kirchhoff migration and a full two-way 3D migration of the Blessing survey

(a). Fault analysis for Kirchhoff depth slice

(b). Fault analysis for two-way depth slice

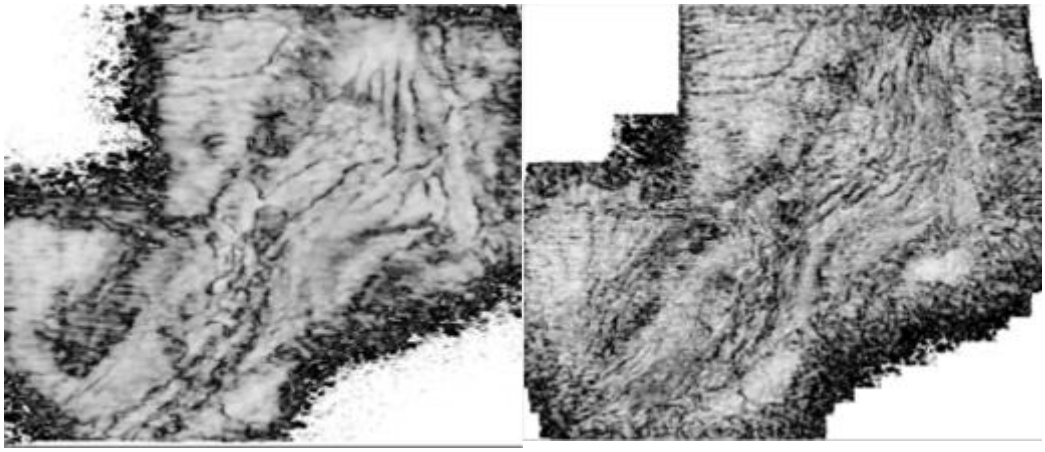

Figure 12-24 is another high-resolution fault analysis at a slightly different depth. The two-way still shows much higher resolution than the Kirchhoff.

Figure 12-24. A high resolution fault analysis of a second set of depth slice from the Blessing data volume.

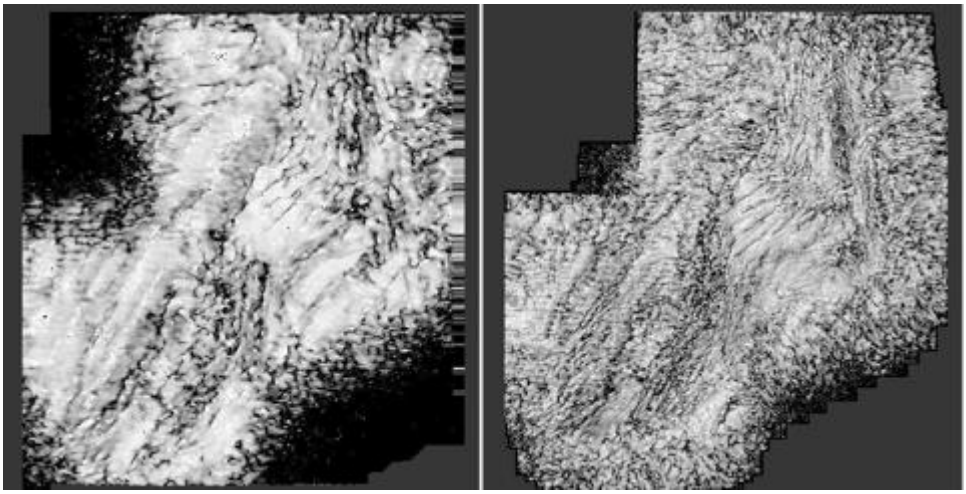

Data Mapping through AMO on the Blessing data

In this section, we consider the utilization of AMO as a data mapping technique. The idea is to construct large aperture rectangular densely sampled shots from either narrow azimuth or widely spaced receiver lines. Figure 12-25(a) shows an AMO based process for construction of large densely sampled areal array shots from otherwise narrow azimuth or widely spaced receiver arrays.

Figure 12-25. Regularization of land data to form a 3D wide azimuth shot.

(a). AMO as data mapping to regularize a 3D shot

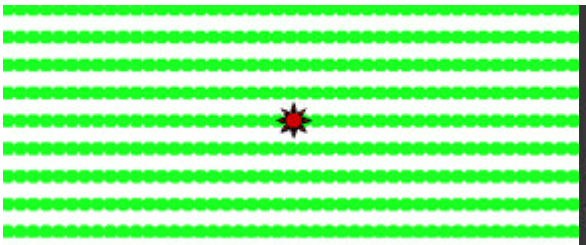

Method 1 - Regularize to output receiver grid
Fixed shot position
Offsets based on output receiver position
Method 2 - Regularize to output midpoint grid
Fixed shot position
Offsets based on output midpoints

(b). Objective fault image

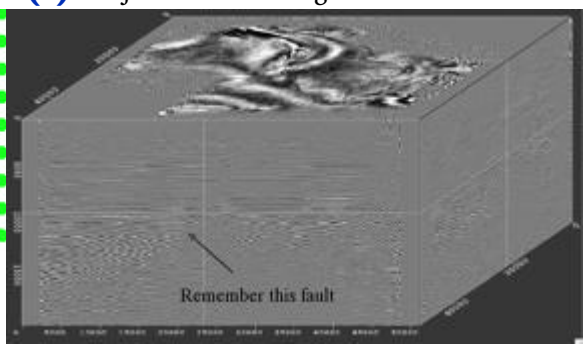

(c). AMO regularized 3D shot

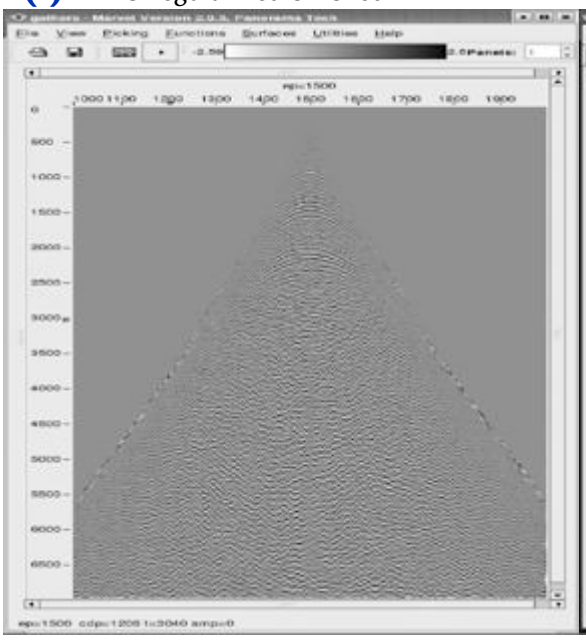

(d). Migrated regularized shot

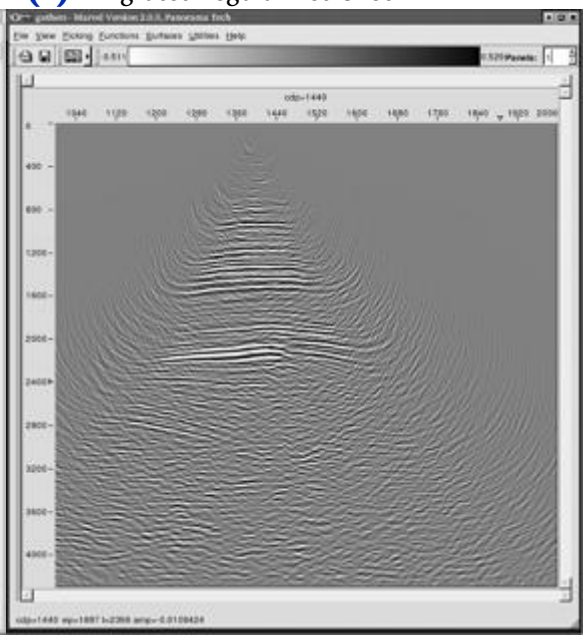

AMO in either FK, as described in previous sections, or in integral form as described by Biondi, *et al.*, can be used to directly construct output volumes of any offset and any azimuth. This can be done trace by trace or by computing all volumes at once. In any case, the data is sorted into common shot volumes and migrated shot by shot. Each migrated shot is a full 3D volume and, according to theory, should provide a superior image. Part (b) of this figure is a simple reminder of the fault that we wish to image. Part (c) shows a slice through a 3D rectangular and densely sampled shot generated to provide a reasonable image of the fault in (b). Part (d) shows that this process, at least for this land data set, is quite successful. There is no doubt that the fault is imaged quite well.